Journal of Hazardous Materials 464 (2024) 132998

Contents lists available at ScienceDirect

Journal of Hazardous Materials

journal homepage: www.elsevier.com/locate/jhazmat

Research Paper

Behavior of ^{222}Rn, ^{220}Rn and their progenies along a daily cycle for different meteorological situations: Implications on atmospheric aerosol residence times and Rn daughters' equilibrium factors

A. Barba-Lobo [a,c,*], I. Gutiérrez-Álvarez [a], J.A. Adame [b], E.G. San Miguel [a], J.P. Bolívar [a]

[a] Radiation Physics and Environment Group (FRYMA), Center for Natural Resources, Health and Environment (RENSMA), University of Huelva, 21007E Huelva, Spain
[b] Atmospheric Sounding Station – El Arenosillo, Atmospheric Research and Instrumentation Branch, National Institute for Aerospace Technology (INTA), Mazagón, Huelva, Spain
[c] Department of Medical Radiation Sciences, Institute of Clinical Sciences, Sahlgrenska Academy at University of Gothenburg, Gothenburg SE-413 45, Sweden

HIGHLIGHTS

- Temporal evolutions of ^{222}Rn, ^{220}Rn, their progenies and their disequilibria were obtained along 24 h cycles.
- Comparisons of their temporal evolutions were made between different meteorological situations.
- The ^{214}, ^{212}Pb and ^{214}, ^{212}Bi were measured by gamma-ray spectrometry each 3 h, using an ASS-500 for aerosol samplings.
- Relationships between the concentrations of radionuclides and meteorological variables of interest were found.
- Aerosol residence times and Rn-daughters' equilibrium factors were obtained along each cycle, finding consistent results.

GRAPHICAL ABSTRACT

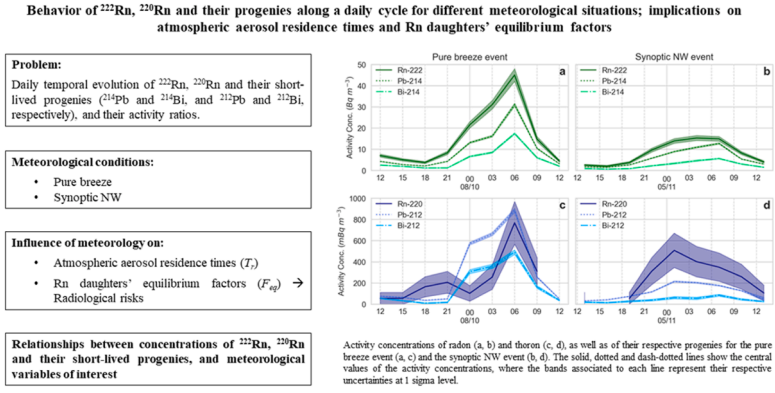

Activity concentrations of radon (a, b) and thoron (c, d), as well as of their respective progenies for the pure breeze event (a, c) and the synoptic NW event (b, d). The solid, dotted and dash-dotted lines show the central values of the activity concentrations, where the bands associated to each line represent their respective uncertainties at 1 sigma level.

ARTICLE INFO

Editor: Lingxin Chen

Keywords:
^{222}Rn – ^{214}Pb – ^{214}Bi
^{220}Rn – ^{212}Pb – ^{212}Bi
Synoptic–mesoscale processes
Residence times
Equilibrium factors

ABSTRACT

The correct assessment of the radiological hazard from radon and daughters, external and internal doses, residence times and equilibrium factors, implies the need to properly determine ^{222}Rn (radon), ^{220}Rn (thoron) and their respective short-lived progenies (^{214}Pb and ^{214}Bi, and ^{212}Pb and ^{212}Bi, respectively), where the precise measurements of both progenies are quite complex due to their very short half-lives. In addition, it is important to study the temporal behavior of all these radionuclides along daily cycles. Therefore, the aim of this study was to analyze the temporal evolution of radon, thoron and their progenies, and of their activity ratios along daily cycles for two different meteorological situations (synoptic and mesoscale processes). Radon and thoron were measured using a radon monitoring system, while their respective progenies were collected onto atmospheric filters using an ASS-500 sampler, and then measured by gamma-ray spectrometry. Furthermore, the different relationships between the concentrations of radionuclides and the different meteorological variables of interest (temperature, ABL height, and speed and direction of the wind) were found. Finally, the atmospheric aerosol

* Corresponding author at: Radiation Physics and Environment Group (FRYMA), Center for Natural Resources, Health and Environment (RENSMA), University of Huelva, 21007E Huelva, Spain.
E-mail addresses: alejandro.barba@dci.uhu.es, alejandro.barba-lobo@gu.se (A. Barba-Lobo).

https://doi.org/10.1016/j.jhazmat.2023.132998
Received 25 August 2023; Received in revised form 31 October 2023; Accepted 11 November 2023
Available online 15 November 2023

residence times and Rn daughters' equilibrium factors were estimated for each sampling carried out along the two daily cycles, finding results consistent with previous studies.

1. Introduction

Radon (^{222}Rn, $T_{1/2}$=3.8 d) and thoron (^{220}Rn, $T_{1/2}$=55.6 s) belong to ^{238}U- and ^{232}Th-series, respectively. Radon and thoron are noble gases produced by decay of ^{226}Ra and ^{224}Ra, respectively. These gases can leave the Earth crust either by molecular diffusion or by convection and enter the atmosphere, where they are distributed by meteorological processes [1]. Due to its relatively long half-life, radon is widely dispersed in the atmosphere. On the contrary, the short half-life of thoron does not allow a large-scale transport. Radon has four short-lived decay products: ^{218}Po (3.05 min), ^{214}Pb (26.8 min), ^{214}Bi (19.7 min), and ^{214}Po (164 μs). Both polonium isotopes are alpha emitters. Relevant thoron daughters for dosimetric measurements are ^{212}Pb (10.6 h) and ^{212}Bi (60.6 min) [2].

It is well known that radon and its progeny are the main source of ionization in the lower troposphere, as well as the main natural source of equivalent dose to the public [3]. Radon and its short-lived radon decay products contribute up to 50 % of the radiation dose delivered to the human lung of all natural sources of radiation [2]. The inhalation of radon decay products depends on their concentrations in air, as well as on their size. There are two forms of radon decay products: the unattached and attached fractions, whose equivalent diffusion diameters are 0.5–5 nm and 5–3000 nm, respectively [4].

Parameters such as the equilibrium-equivalent concentration of airborne radon progeny, unattached fraction and equilibrium factor are among the most important input parameters in dosimetric models to determine exposure and radiation dose by inhalation [5,6]. The equilibrium factor (F_{eq}) allows the exposure to be estimated in terms of (PAEC) from the measurements of radon gas concentration. The F_{eq} is defined as the ratio of the measured potential alpha energy concentration (PAEC), which occurs when all radon decay products are in secular equilibrium with the measured ^{222}Rn [7]. The PAEC is the sum of the alpha particle decay energy of all the short-lived progeny of radon in a volume of air (J m^{-3}). In the case of ^{222}Rn and ^{220}Rn progenies, the equations to calculate their equilibrium factors (F_{eq}(^{222}Rn) and F_{eq}(^{220}Rn), respectively) are well known and they can be consulted elsewhere [8]. Thoron equilibrium factor varies significantly even for the same environment mainly due to wide variations of thoron concentration arising from its short-lived nature.

The residence time of aerosols is an important parameter that provides a measure of how far a released substance to the atmosphere is deposited on the soils [9]. The residence time can be calculated using the short-lived ^{222}Rn and ^{220}Rn progenies assuming steady state between the production and removal rates and using a box model [10]. In the case of the ^{220}Rn progeny, T_r can be obtained by means of the ^{212}Bi/^{212}Pb activity ratio [11]. Nevertheless, for the estimation of mean residence times from ^{222}Rn progeny, it is preferable using ^{214}Pb/^{222}Rn activity ratio instead of ^{214}Bi/^{214}Pb activity ratio, since the half-lives of ^{214}Bi and ^{214}Pb are similar to each other [12].

In addition, radon and thoron have been used as tracers for different atmospheric processes [1,13,14], hydrogeological and geological processes [15] and other environmental applications [16].

Lead-214, 212 and ^{214,212}Bi are essential to assess external and internal doses, radiological hazard, residence times and equilibrium factors. However, due to their very short half-lives, precise determinations of these radionuclides are very difficult [11]. Thoron progeny, ^{212}Pb and ^{212}Bi, which dominantly contribute to the equilibrium equivalent thoron concentration, are beta emitters and can be measured by gamma-ray spectrometry. Radon daughters, ^{214}Pb and ^{214}Bi, emit beta particles and gamma rays with high branching ratios.

Two 24 h sampling cycles with quite different meteorological situations (mesoscale and synoptic) were selected to analyze the temporal evolution of radon, thoron and their respective progenies. For the first meteorological situation, mesoscale winds (pure breeze in our case) were present, and for the second meteorological situation, N/NW synoptic winds coming from the Atlantic Ocean were present.

The aim of this work was to develop a high time resolution study (one measurement every 3 h) to analyze the influence of different meteorological situations on the concentrations of radon, thoron, and their progenies, along a typical day under two different meteorological situations. Specifically, the present study allows quantifying the influence of several meteorological variables such as temperature (T), wind speed and direction (WS and WD, respectively), and the height of the atmospheric boundary layer (ABL), on the concentrations of radon, thoron, and their progenies throughout a daily cycle for the two meteorological situations.

To the best of our knowledge, this is the first study to thoroughly address the temporal evolution of radon, thoron and their respective short-lived progenies outdoors for two complete 24 h sampling cycles, considering two different meteorological situations, and employing an ASS-500 for samplings and gamma-ray spectrometry to measure radon and thoron short-lived progenies. Furthermore, the dependence of the concentrations of each radionuclide on several meteorological variables of interest was analyzed for both cycles, and the methodology, which was employed to determine radon, thoron and their respective short-lived progenies, was applied to estimate atmospheric aerosol residence times and Rn daughters' equilibrium factors, whose temporal evolutions were also analyzed for both cycles considered in this study. Due to the very high complexity of carrying out measurements of the radon and thoron short-lived progenies by gamma-ray spectrometry for a complete 24 h cycle, where their measurements were carried out every 3 h, a day was selected for each 24 h cycle. Thus, the results obtained in this study can be generalized to other geographical areas with similar meteorological situations to those considered in this study, that is, synoptic or mesoscale processes such as N/NW winds and pure breezes, respectively. Therefore, the results presented in this article on the meteorological influence on the temporal evolution of radon, thoron and their short-lived progenies, as well as on the atmospheric aerosol residence times and Rn daughters' equilibrium factors, can have a generalized applicability.

2. Study area description, materials and methods

2.1. Study area

The study area focuses on the city of Huelva, situated in the Southwest of the Iberian Peninsula (Fig. 1a), bordered by the Tinto and Odiel rivers, close to the Atlantic Ocean and in the mouth of the Guadalquivir valley. The atmospheric dynamics in this region are characterized by a combination of synoptic and mesoscale processes. The synoptic airflows can have both a maritime or continental origin. Regarding maritime air masses coming directly from the Atlantic Ocean and continental air masses, they can have a double origin: from the interior of the Iberian Peninsula or North Africa. In situations with a weak isobaric gradient, mesoscale processes take place, such as sea-land breezes. In previous works, two types of sea-land breezes have been identified: i) a pure breeze, with a wind direction perpendicular to the coastline, and ii) a non-pure breeze, which results from the flow of the former and Northwesterly synoptic forcing [17]. These two meteorological situations (N/NW synoptic winds and pure breezes) were selected, based on the fact that they are very different from each other, which makes it possible to properly analyze the influence of meteorology on the temporal

behavior of the radionuclides of interest. Moreover, the two selected meteorological situations are very representative and typical of the Huelva province, which has been proved in previous studies carried out in this region [17,18], which further justifies their selection.

For this study, El Carmen campus (at Huelva province) was selected as the study area. In addition to the air samplers, the laboratory of detectors is located in El Carmen campus, which allowed carrying out the measurements of filters as soon as possible after the sampling ended, in order to precisely measure the short-lived progenies of radon and thoron. Furthermore, from a meteorological point of view, Huelva province is characterized by having meteorological situations that are very different from each other such as synoptic winds and pure breezes. This is very proper for the analysis of the influence of the different meteorological situations on the temporal evolution of radon, thoron and their respective short-lived progenies, as well as on the temporal evolution of the atmospheric aerosol residence times and Rn daughters' equilibrium factors. Moreover, due to several studies carried out in Huelva province [17,18], the meteorological situations typically present in Huelva province are well known, which is another reason to select Huelva province as the study area.

2.2. Samplings

Surface air aerosols were collected at El Carmen campus of Huelva University (37°16'12''N 6°55'28''W) in Huelva (Spain). The sampling altitude was 6 m above the ground. Surface air samples were collected using a high-volume aerosol sampler, model ASS-500, with flows ranging from 500 $m^3\ h^{-1}$ to 600 $m^3\ h^{-1}$ (details on ASS-500 sampler in [19]). Samples were collected with polypropylene filters (44 × 44 cm^2), whose collection efficiency was higher than 93%.

Based on the previous studies in the area [17], two 24 h sampling cycles with different weather conditions were selected to analyze the temporal evolution of radon, thoron and their respective progenies. The first 24 h cycle was from October 7, 2021 at 12:00 UTC to October 8, 2021 at 12:00 UTC, which was characterized by mesoscale processes (pure breezes). The second 24 h cycle was from November 4, 2021 at 13:00 UTC to November 5, 2021 at 13:00 UTC; in this period, the atmospheric dynamics were governed by synoptic airflows coming from N/NW. For each 24 h cycle, a total of 9 samplings were collected. The sampling period was 1 h, and the time elapsed between samplings was 2 h.

2.3. Measuring techniques and quality control

The measurements of ^{212}Pb, ^{212}Bi, ^{214}Pb and ^{214}Bi were carried out by gamma-ray spectrometry, using an extended range (XtRa) HPGe detector. The XtRa detector has a relative efficiency of 38.4% at 1332 keV (^{60}Co) (with respect to a 3″ × 3″ NaI (Tl) detector), a full width at half maximum of 1.74 keV and 0.88 keV at 1332 keV and 122 keV, respectively, and a peak-to-Compton ratio of 67.5:1. The XtRa detector is connected to a device for the data acquisition and the gamma spectra visualization using the Genie 2000 software [20]. This detector was shielded with a Fe layer of 15 cm thickness, internally with a thin Pb layer. A layer of 2 mm thick Cu plate was placed on the top of the Pb layer to avoid the interferences from Pb X-ray in the obtained gamma spectra.

For the XtRa efficiency calibration, polypropylene 44 × 44 cm^2 filters were used. Certified reference materials (CRMs) provided by the IAEA (International Atomic Energy Agency), whose codes are RGU-1 and RGTh-1, were selected. They contain only natural radionuclides belonging to the ^{238}U- and ^{232}Th-series, respectively, whose reference activity concentrations are 4940(15) Bq kg^{-1} and 3250(45) Bq kg^{-1}, respectively. These CRMs were well mixed and uniformly spread on three calibration filters, reproducing the same geometry as that of the sample collection. Then, they were folded with the same dimensions as those used for the measurements of any problem filter (11 ×11 cm^2). Afterwards, they were pressed to obtain a small thickness, avoiding the need for correcting self-absorption effects when obtaining the full-energy peak efficiency (*FEPE*) at energies of interest. Finally, the filters were inserted into plastic bags and vacuum was applied to keep the geometrical efficiency constant. Three filters were selected for the efficiency calibration to verify the reproducibility of the efficiency obtained for each selected energy. The detector was calibrated with the same radionuclides of interest in this study (^{214}Pb (352 keV), ^{214}Bi (609 keV), ^{212}Pb (238 keV) and ^{212}Bi (via ^{208}Tl (583 keV)). The detailed procedure of efficiency calibration of polypropylene filters, as well as the determinations of ^{212}Pb, ^{212}Bi, ^{214}Pb and ^{214}Bi, are published elsewhere [11,21].

For the measurements of ^{222}Rn and ^{220}Rn, a measurement system was settled at the same place chosen for the ASS-500 sampler. This system is based on Atmospheric Radon Monitoring (ARMON), which is composed of a Passivated Implanted Planar Silicon (PIPS) detector inside a 20 L spherical detection volume, establishing a potential difference of 8000 V between the inner layer of the sphere and the PIPS detector. In the ARMON system, the PIPS detector detects α-particles resulting from ^{216}Po and ^{218}Po decays, from the thoron and radon,

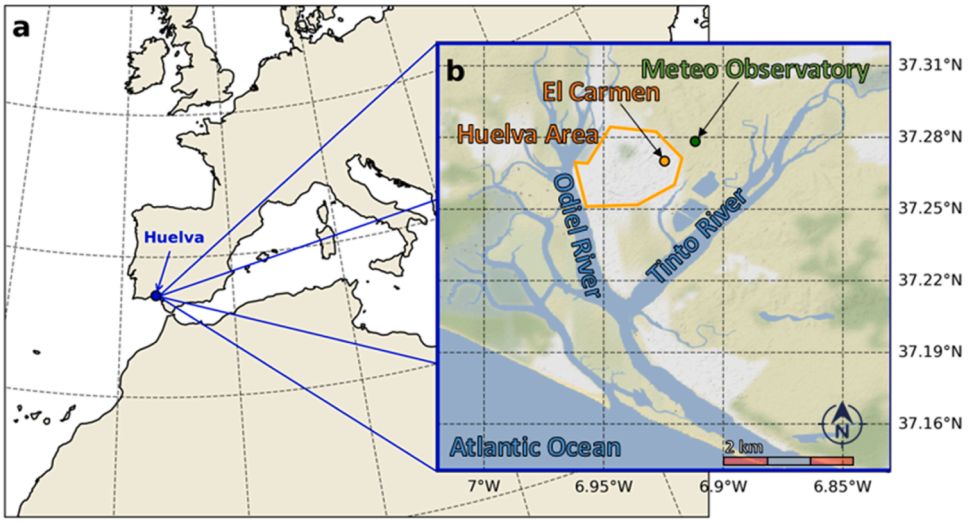

Fig. 1. a) Location of Huelva city in Europe. b) Huelva measurement station (El Carmen), Meteorological Observatory and Huelva city area.

respectively. The ARMON system has a 1 μm filter which is placed at sphere entrance to trap all thoron and radon daughters, which are generated before entering this sphere. The minimum detectable activity concentration (*mda*) was about 50 mBq m^{-3} and 200 mBq m^{-3} for thoron and radon, respectively. Further information about the ARMON system employed in this study, its calibration, and its calibration validation can be consulted in previous studies [22–25].

Quality control of measurements was carried out through participation in inter-comparison exercises using this type of filters for natural and artificial radionuclides with satisfactory results. Detailed results on the inter-comparison exercises can be found in Barba-Lobo and Bolívar [21].

2.4. Meteorological models and computation of trajectories

The local weather conditions were analyzed with the meteorological observations obtained in a meteorological observatory located 1.5 km from the sampling site (Fig. 1b). This station provides surface data of temperature, relative humidity, pressure, and wind (speed and direction) with a time resolution of 10 min, which were hourly averaged in this study for their comparison with radon measurements.

To identify air masses pathways during the two samplings, back trajectories were computed using the HYSPLIT (Hybrid Single-Particle Lagrangian Integrated Trajectory) model developed by the Air Resources Laboratory at NOAA (National Oceanic and Atmospheric Administration) [26]. Hourly three-dimensional back trajectories were used with a 24-h pathway at 100 m a.g.l. ERA5 data reanalysis from the ECMWF (European Centre for Medium-Range Weather Forecast) model was used to calculate the trajectories. ERA fields show a horizontal spatial resolution of 0.25 degrees and 37 vertical pressure levels [27]. ERA5 was also used to obtain the atmospheric boundary layer (ABL) height, in order to determine the stable or unstable vertical conditions during the samplings.

3. Results and discussion

This section is also divided into four subsections. The first section explains each of the analyzed meteorological situations. The second section analyzes the temporal evolution of radon, thoron and their short-lived progenies concentrations throughout the daily cycle in each sampling period. The third section explores the relationship between radon and thoron concentrations and different meteorological variables. Lastly, the fourth section shows several applications, such as residence time and radon daughters' equilibrium factors calculations.

3.1. Weather conditions of the samplings

The temporal evolution of the surface meteorological parameters registered in each sampling is shown in Fig. 2. The first sampling was conducted under weak synoptic conditions, which allowed for the development of a pure breeze pattern, typical of the area [17]. This type of breeze is characterized by Southwest (SW) winds, of maritime origin, in diurnal regime, followed by a change of direction towards Northeast (NE) during nighttime hours, with airflows coming from inland. At the beginning of the sampling, wind speeds were between 2.5 and 5 m s^{-1}, staying under 2 m s^{-1} between 21:00 UTC on October 7 and 9:00 UTC on October 8, and increasing up to 4 m s^{-1} afterwards. ABL height was under 450 m during the entire sampling, describing a pattern that was analogous to that of wind speed, staying under 200 m between 18:00 UTC on October 7 and 9:00 UTC on October 8. Temperature and specific humidity follow a classical pattern with higher temperatures and lower humidities at 12:00 UTC, and the opposite situation immediately before sunrise, at 6:00 UTC in the morning on October 8.

The atmosphere during the second sampling was governed by synoptic conditions, i.e., forcing winds from Northwest-North (NW-N) for most of the day. In this case, wind speeds were around 4 m s^{-1} at 13:00 UTC on November 4, slowly decreasing until reaching 2 m s^{-1} at 18:00

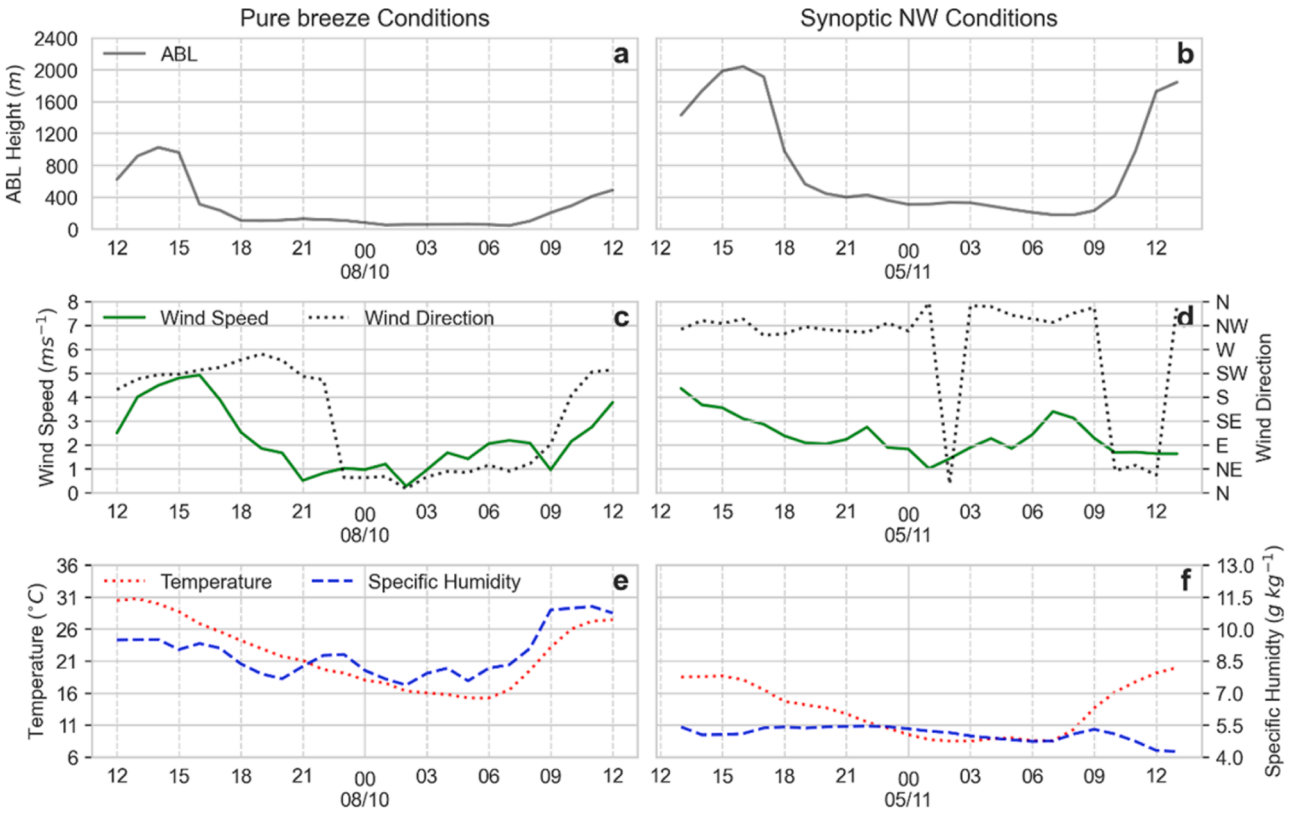

Fig. 2. Temporal evolutions for ABL height (a-b), wind (speed and direction) (c-d), temperature and specific humidity (e-f), under the pure breeze sampling from October 7–8, 2021 (a, c, e), and for the synoptic NW event, November 4–5, 2021 (b, d, f).

UTC on November 4, remaining stable until sunrise on November 5 at around 6:00 UTC. ABL height was significantly higher at the beginning of the sampling, being above 1000 m from 12:00 UTC to 18:00 UTC on November 4, and decreasing to a constant level of 300–400 m until 9:00 UTC on November 5. Finally, temperature and specific humidity followed a typical diurnal pattern, with higher values for temperature and lower values for humidity at noon (20 °C and 10 g kg^{-1}, respectively), and inverted conditions during nighttime (minimum temperature around 10 °C and maximum specific humidity ~ 17 g kg^{-1}).

Note that, in Fig. 2, for the same meteorological variable, the same scale was selected for both meteorological conditions to carry out the comparisons adequately. For the other figures (from Fig. 3 to Fig. 8), the same procedure was followed.

To analyze the origin of the air masses arriving to the study area, the back-trajectories were computed (Fig. 3). During the first sampling, due to the development of sea-land breeze, the air masses remained in the previous 24 h in the local area, which is in line with the breeze pattern discussed above. Between 24 h and 48 h prior to the sampling, they reached mainly areas in the Alborán Sea, the Mediterranean Sea, and some areas around the center of Spain and Portugal. From 48 h to 72 h prior to the sampling, only some of the trajectories reached the Atlantic Ocean on the West, most of them still travelling over the Iberian Peninsula and another group coming from the Mediterranean Sea to the East.

The second sampling showed classical synoptic forcing conditions, with most of the air masses coming from the area of the Atlantic Ocean to the West of the British Islands, thus having a North Atlantic Ocean origin. These air masses travelled fast, only being over the Iberian Peninsula for the 24 h prior to the sampling and spending most of the period of 24–48 h prior to the sampling over the Atlantic Ocean. The last period of 24 h (48–72 h) was divided into two clear groups: one travelled over Ireland and the other group passed over open sea to the Western British Islands.

3.2. *Temporal evolution of ^{222}Rn, ^{220}Rn and their short-lived progenies*

Fig. 4 shows the activity concentrations measured for radon, thoron and their progenies. For both 24 h cycles, the temporal behaviors of the progenies of radon and thoron are very similar to those followed by their respective parents (Fig. 4a and b, respectively), which is in agreement with the results of previous works [1]. For the first cycle, the concentrations clearly reached the maximum values at about 6:00 UTC (41(3) Bq m^{-3}, 31.0(7) Bq m^{-3} and 17.4(4) Bq m^{-3} for ^{222}Rn, ^{214}Pb and ^{214}Bi, respectively, and 767(202) mBq m^{-3}, 884(20) mBq m^{-3} and 491(22) mBq m^{-3} for ^{220}Rn, ^{212}Pb and ^{212}Bi, respectively, where the uncertainties at 1 sigma level were written between parenthesis). This is due to the fact that, at 6:00 UTC, the sunrise takes place at Huelva province in the month of October. At 6:00 UTC, the tendency of the temperature and absolute humidity changes, as can be observed in Fig. 3, the sunlight starts to warm the soil and vertical air movement ensues, allowing for the mixing of radon and its daughters in a greater volume of air [28]. Tables A.1 and A.2 in Supplementary Material (Appendix A) provide detailed information about the activity concentrations obtained for ^{220}Rn-progeny and ^{222}Rn-progeny, respectively, corresponding to the first sampling cycle.

However, in the case of the second cycle (synoptic NW), the temporal evolution of radon, thoron and their progenies follows the typical daily behavior, although reaching lower values than those found for the first cycle (pure breeze). The maximum activity concentrations reached for the second cycle are much lower than those obtained for the first cycle (about 3 and 4 times lower for ^{222}Rn-progeny and ^{220}Rn-progeny, respectively). This result could be related to the origin of the air masses, since, under pure breeze conditions, the air masses spent longer times in the local area, allowing for the enhancement of radon concentration, whereas, under synoptic NW, air masses travelled quickly from the Atlantic Ocean, spending most of their time above the sea without a radon source nearby. Tables A.5 and A.6 in Supplementary Material (Appendix A) show detailed information about the activity concentrations obtained for ^{220}Rn-progeny and ^{222}Rn-progeny, respectively, for the second sampling cycle.

Regarding the activity ratios found for each 24 h cycle, it is possible to observe that, for each couple of radionuclides, their activity ratios were relatively stable throughout the entire 24 h cycle. This means that the secular disequilibrium found for each couple of radionuclides remained almost constant regardless of the different values obtained for the meteorological variables. For radon and its progeny (Fig. 5a), the average ^{214}Pb/^{222}Rn activity ratios were found to be 0.61(3) and 0.70(2) for pure breeze and synoptic NW conditions, respectively, where the

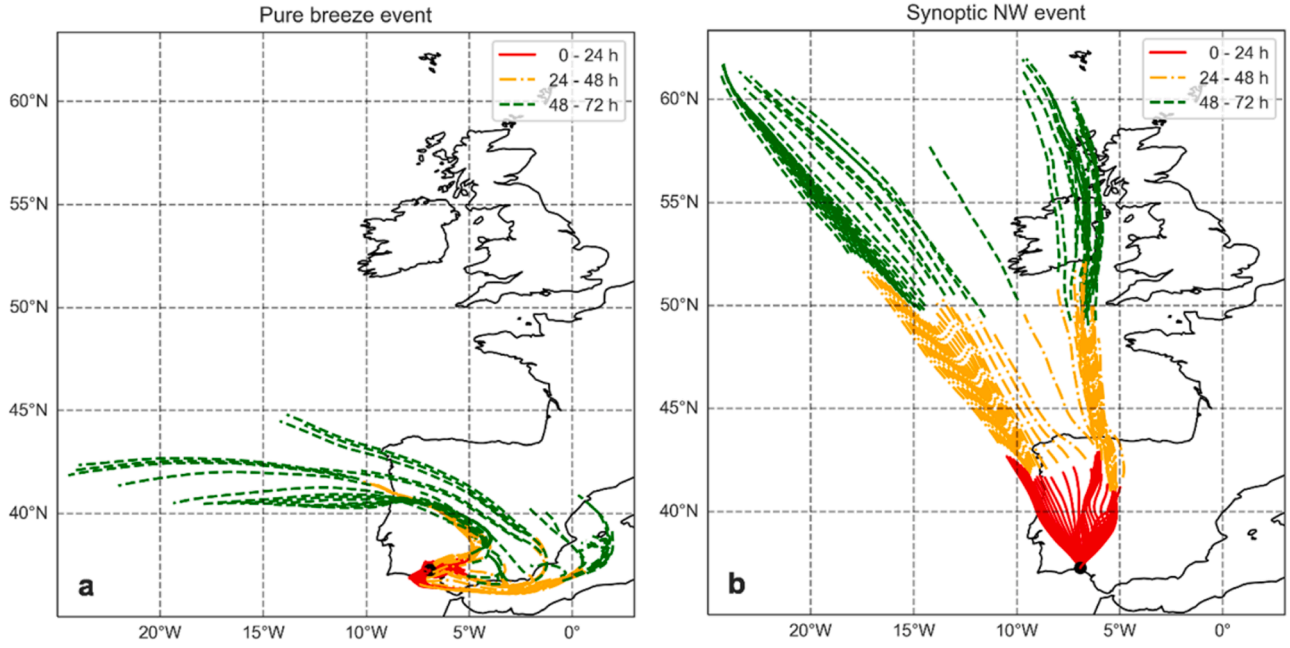

Fig. 3. Hourly back trajectories computed with HYSPLIT model using ERA5 meteorological fields with 24 h pathways at 100 m a.g.l from October 7–8, 2021 under pure breeze event (a) and from November 4–5, 2021 under synoptic NW event (b).

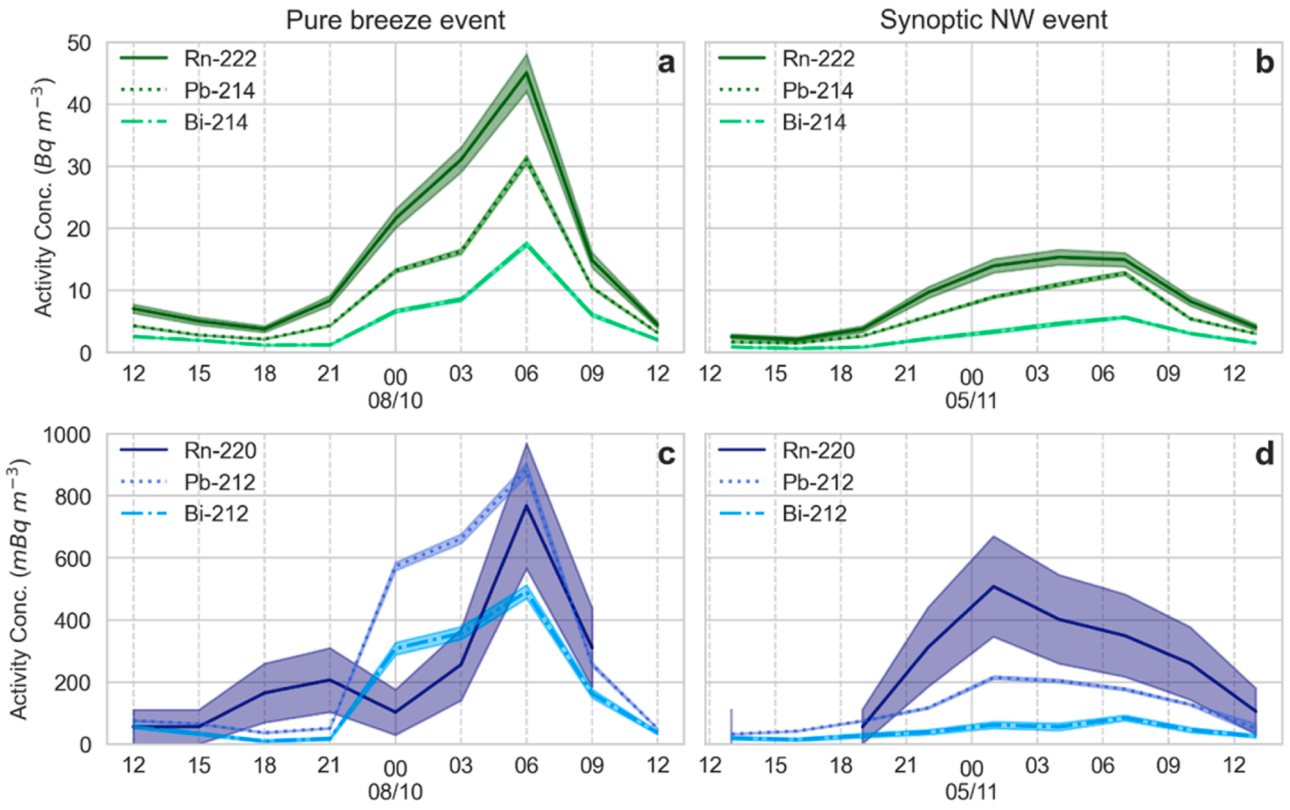

Fig. 4. Activity concentrations of radon (a, b), thoron (c, d) and their respective progenies for the pure breeze event (a, c) and the synoptic NW event (b, d). The solid, dotted and dash-dotted lines show the central values of the activity concentrations, where the bands associated with each line represent their respective uncertainties at 1 sigma level.

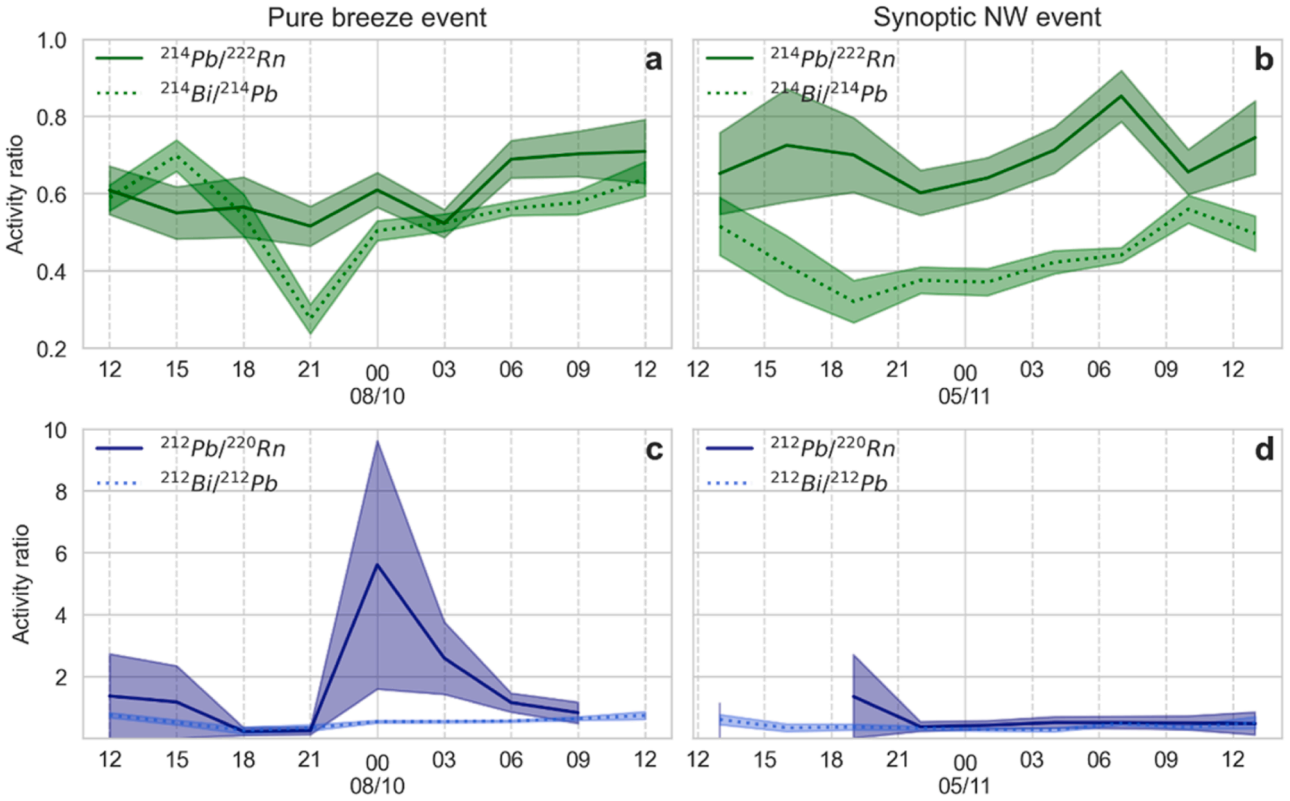

Fig. 5. Activity ratios of $^{214}Pb/^{222}Rn$, $^{214}Bi/^{214}Pb$ (a, b), $^{212}Pb/^{220}Rn$ and $^{212}Bi/^{212}Pb$ (c, d), obtained for the pure breeze event (a, c) and the synoptic NW event (b, d).

standard deviation of the mean is expressed between parentheses. Their relative uncertainties were 5% and 3%, respectively, indicating that the $^{214}Pb/^{222}Rn$ activity ratios remained stable during both cycles. In the case of $^{214}Bi/^{214}Pb$, the average activity ratios were 0.55(4) and 0.44(3) for pure breeze and synoptic NW conditions, respectively, with a relative uncertainty of 7% for both cases.

Consequently, it is also possible to observe that the behavior of $^{214}Bi/^{214}Pb$ did not show significant variations for any of the cycles. This result could be expected, since, during each of the 24 h sampling cycles, the air mass stayed in the area (Fig. 3) and, consequently, disequilibrium between the different couples of radionuclides remained almost constant during both sampling periods. Regarding the comparison of the activity ratios obtained for the different meteorological situations, these were not statistically compatible. In order to compare the activity ratios between the sampling periods, a *t*-paired test was performed. The |*t*-test| values obtained for $^{214}Pb/^{222}Rn$ and $^{214}Bi/^{214}Pb$ activity ratios were 3.4 and 2.9, respectively, while the critical *t*-test was 2.3 (significance level of 5%, 8 degrees of freedom) for both activity ratios. Consequently, the activity ratios obtained during each cycle were significantly different at 5% level. This could be due to the different origin and paths of the air masses arriving to the sampling site for each meteorological situation. Therefore, the sources of radionuclides feeding these air masses also differ, leading to different degrees of disequilibrium between them.

In the case of thoron and its progeny (Fig. 5b), similar results were obtained. For the ^{212}Pb-^{220}Rn couple, their average activity ratios were 1.7(6) and 0.7(2) for pure breeze and synoptic NW conditions, respectively, whose relative uncertainties were 35% and 29%, respectively. These high relative uncertainties are due to the complexity of measuring thoron outdoor levels. However, as is shown in Fig. 4, ^{220}Rn-progeny follows the same behavior as ^{222}Rn-progeny, which can be corroborated

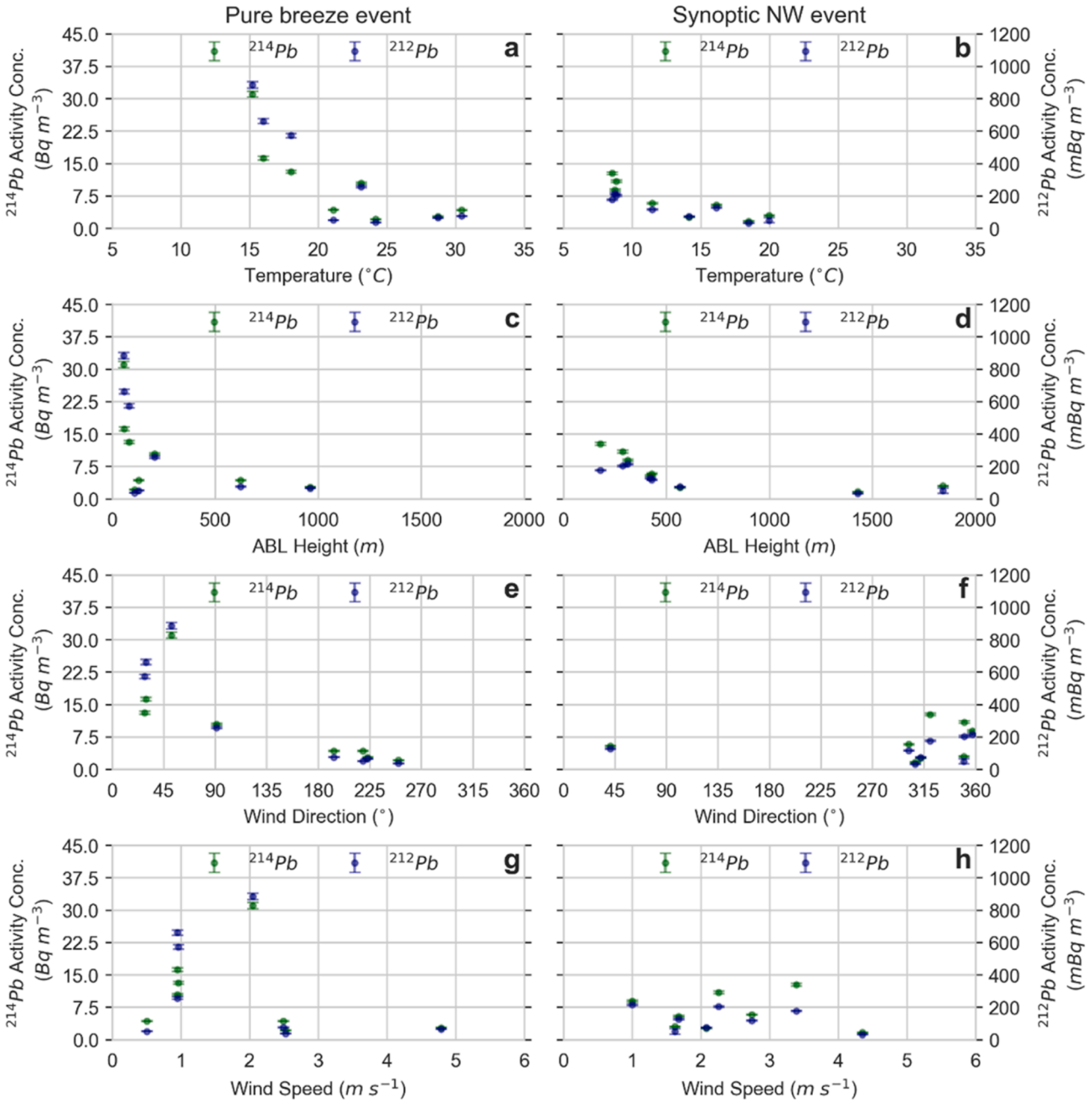

Fig. 6. Dependence of the activity concentrations of ^{214}Pb and ^{212}Pb on several meteorological variables such as temperature (a, b), height of the atmospheric boundary layer (c, d), wind direction (e, f), and wind speed (g, h) for the pure breeze event (a, c, e, g) and the synoptic NW event (b, d, f, h).

with other studies [29]. Therefore, for the same 24 h cycle, the secular disequilibria between ^{220}Rn and ^{212}Pb can be assumed to be also very stable. For the ^{212}Bi-^{212}Pb couple, the average activity ratios were 0.54 (5) and 0.39(4) for pure breeze and synoptic NW conditions, respectively, whose relative uncertainties were 9% and 10%, respectively. This is in line with the results shown in Fig. 5a, indicating the feasibility of considering that the ^{212}Pb/^{220}Rn activity ratio remains almost constant during both samplings cycles.

When comparing the activity ratios of ^{222}Rn-progeny radionuclides between both cycles through the *t*-paired test, the values obtained for ^{212}Pb/^{220}Rn and ^{212}Bi/^{212}Pb activity ratios were 1.6 and 3.5, respectively, whereas the critical *t*-test was 2.3. In the case of the ^{212}Pb-^{220}Rn couple, the fact that the *t*-test value was lower than the critical value could be due to the relatively high standard deviation obtained for this case. Applying the *F*-Fisher test to analyze the statistical compatibility between the variances of the ^{212}Pb-^{220}Rn couple at 5% significance level, Fisher's *F* was 12.9 for the ^{212}Pb/^{220}Rn activity ratios, whereas critical Fisher's *F* was 3.4. Therefore, for the same couple of radionuclides, the activity ratios obtained for both cycles were not statistically compatible, which is consistent with the findings of the ^{222}Rn-progeny.

3.3. Radon behavior with different meteorological variables and conditions

To analyze the behavior of the radon and thoron daughters versus the most significant meteorological parameters, a Principal Component Analysis was conducted, with the correlation matrix being included in Tables B.1 and B.2 (in Supplementary Material, Appendix B). In these tables, the significant correlation coefficients with p-values < 0.05 are shown in bold letter.

Significant correlation coefficients were found for temperature with radon and thoron progenies, with negative correlations for both ^{214}Pb and ^{212}Pb (r = - 0.83 and - 0.63, respectively). This could be due to the fact that temperature is generally lower during the night, the ABL height decreases and, therefore, the dispersion of radon and thoron also decreases. As can be observed in Fig. 6, in each of the meteorological conditions, the concentrations of these radionuclides increase during the night, leading to concentrations that are one order of magnitude higher than those obtained during the hours corresponding to the highest temperatures.

With respect to wind direction (WD), two sets of concentration values were observed under pure breeze conditions (see Fig. 6). The first group, with the highest concentrations for the sea breeze situation, corresponds to WD = 0–45° (wind from the North, inland), and low wind speed (WS). The second set (lowest values) is given for WD = 180–270° (Southwest or offshore wind), with winds coming from the Atlantic Ocean and, consequently, with lower radon concentrations. Nevertheless, during the synoptic NW event, a wind coming from the Northeast to the North is present (315–360°, inland in every moment), which is very uniform and contains low radon and thoron progeny concentrations, regardless of the wind speed (WS).

It is worth noting the role of the atmospheric boundary layer (ABL), a parameter that indicates the air mixing vertical height. As can be observed in Fig. 6, the lower the ABL height, the higher the radon and thoron daughter concentrations, since the exhalated radon from the surface soil is accumulated in a smaller air volume.

Finally, for further validation of the uniformity of the different activity ratios obtained for the same sampling cycle (see Section 3.2, Fig. 5), a correlation analysis was also carried out for the different couples of radionuclides. Thus, very high correlation coefficients between both ^{222}Rn and ^{220}Rn daughters were found (> 0.90) for both daily cycles. Therefore, for ^{222}Rn progeny and cycle 1, the following fittings were found:

$$^{214}\text{Pb} = (0.65 \pm 0.04)\cdot{}^{222}\text{Rn} - (0.5 \pm 0.9)\ (R^2 = 0.97) \quad (1)$$

$$^{214}\text{Bi} = (0.36 \pm 0.03)\cdot{}^{222}\text{Rn} - (0.3 \pm 0.7)\ (R^2 = 0.94) \quad (2)$$

$$^{214}\text{Bi} = (0.56 \pm 0.02)\cdot{}^{214}\text{Pb} - (0.1 \pm 0.3)\ (R^2 = 0.990) \quad (3)$$

$$^{212}\text{Bi} = (0.548 \pm 0.014)\cdot{}^{212}\text{Pb} - (2 \pm 6)\ (R^2 = 0.996) \quad (4)$$

The fittings found for cycle 2 were:

$$^{214}\text{Pb} = (0.74 \pm 0.06)\cdot{}^{222}\text{Rn} - (0.3 \pm 0.6)\ (R^2 = 0.95) \quad (5)$$

$$^{214}\text{Bi} = (0.30 \pm 0.04)\cdot{}^{222}\text{Rn} - (0.0 \pm 0.4)\ (R^2 = 0.90) \quad (6)$$

$$^{214}\text{Bi} = (0.42 \pm 0.03)\cdot{}^{214}\text{Pb} - (0.1 \pm 0.2)\ (R^2 = 0.96) \quad (7)$$

$$^{212}\text{Bi} = (0.28 \pm 0.06)\cdot{}^{212}\text{Pb} - (2 \pm 6)\ (R^2 = 0.8) \quad (8)$$

The ordinates were statistically compatible with 0 for the four fittings at each meteorological cycle. In addition, for the great majority of the fittings, the relative uncertainties of the slopes were found to be less than 10%. Therefore, the stability of the activity ratios found in Section 3.2 (Fig. 5) is completely proven. The plots of these fittings are included in Supplementary Material (see Figs. B.1 and B.2 in Appendix B). Dissimilar disequilibria (slopes of the fittings) between radon daughters for both daily cycles were found, which is in agreement with the statistical tests previously shown in Section 3.2.

3.4. Applications

Mean aerosol residence times (T_r) and Rn daughters' equilibrium factors (F_{eq}) were estimated based on the methodology developed by Barba-Lobo et al. [11] to precisely measure the short-lived progenies of radon and thoron through gamma-ray spectrometry. In Sections 3.4.1 and 3.4.2, the temporal evolutions of T_r and F_{eq} are analyzed for both 24 h cycles considered in this study.

3.4.1. Aerosol residence times

The temporal evolution of T_r estimated from ^{214}Pb/^{222}Rn and ^{212}Bi/^{212}Pb activity ratios (T_r^{214} and T_r^{212}, respectively) is depicted in Fig. 7. The methodology used to estimate T_r^{214}, T_r^{212} and their respective uncertainties can be found in Barba-Lobo et al. [11].

Thus, for each 24 h cycle, T_r^{214} values were found to be very stable along the entire cycle, achieving average T_r^{214} of 1.25(14) h and 1.9(3) h for pure breeze and synoptic NW conditions, respectively. This can be proven by means of the relative standard deviation of the mean for T_r^{214} for each case, which were 11% and 16%, respectively. This is in line with the behavior of the activity ratios of ^{222}Rn-progeny previously analyzed in Section 3.2. This agreement could be expected due to the relationship between T_r^{214} and the ^{214}Pb/^{222}Rn activity ratio. Furthermore, for the synoptic case, a maximum of T_r^{214} can be clearly observed at 7:00 UTC. This could be explained by using the ^{214}Pb/^{222}Rn activity ratio (see Fig. 5b), whose value was about 0.85 at that time, which is quite higher than the average value found for the ^{214}Pb/^{222}Rn activity ratio in the synoptic case (0.70(2), see Section 3.2). Consequently, given that T_r^{214} is directly proportional to the ^{214}Pb/^{222}Rn activity ratio [11], a notable maximum of T_r^{214} was observed. However, the uncertainty of T_r^{214} is relatively high for this case, making this T_r^{214} value statistically compatible with the other T_r^{214} values found for the same cycle. This is in agreement with the results previously obtained in Sections 3.2 and 3.3, where, for the same cycle, a clear stability was found for the activity ratios of the different couples of radionuclides.

In the case of T_r^{212}, analogous results were obtained, finding average T_r^{212} of 2.1(4) h and 1.03(19) h for pure breeze and synoptic NW conditions, respectively, which have a relative uncertainty of 19%. This is consistent with the behavior found for the ^{212}Bi/^{212}Pb activity ratio (see Section 3.2).

In addition, the T_r^{214} and T_r^{212} values found in this study are in line with those achieved in a previous work [11], where T_r^{214} and T_r^{212} were also ranged from 1 h to 3 h.

See Tables A.3 and A.7 (in Supplementary Material, Appendix A) for

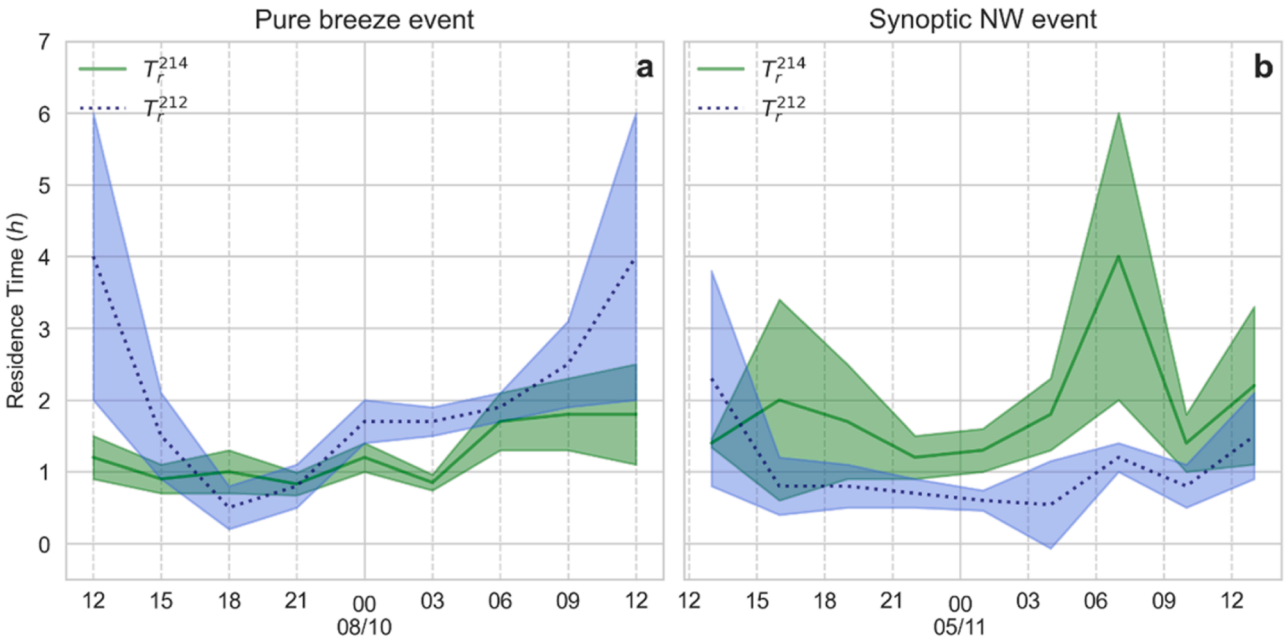

Fig. 7. Residence times (T_r), for ^{212}Bi/^{212}Pb (T_r^{212}) and ^{214}Pb/^{222}Rn (T_r^{214}) obtained by using the *box model* for the pure breeze event (a) and the synoptic NW event (b).

further information about both residence times (T_r^{212} and T_r^{214}) obtained for each sampling carried out during the first and second 24 h cycle, respectively.

3.4.2. *Radon daughters' equilibrium factors*

Radon daughters' equilibrium factors and their uncertainties (Fig. 8) (F_{eq}) for radon and thoron daughters (F_{eq}(^{222}Rn) and F_{eq}(^{220}Rn), respectively) were obtained along the two 24 h cycles, by applying equations provided by Barba-Lobo et al. [11].

For the pure breeze and the synoptic NW events, the average (^{222}Rn) was 0.55(2) and 0.581(19), whose relative standard deviations were 4% and 3%, respectively. Therefore, for the same 24 h cycle, F_{eq}(^{222}Rn) did not have a significant temporal dependence along the entire cycle. This is consistent with the stability found for the different activity ratios

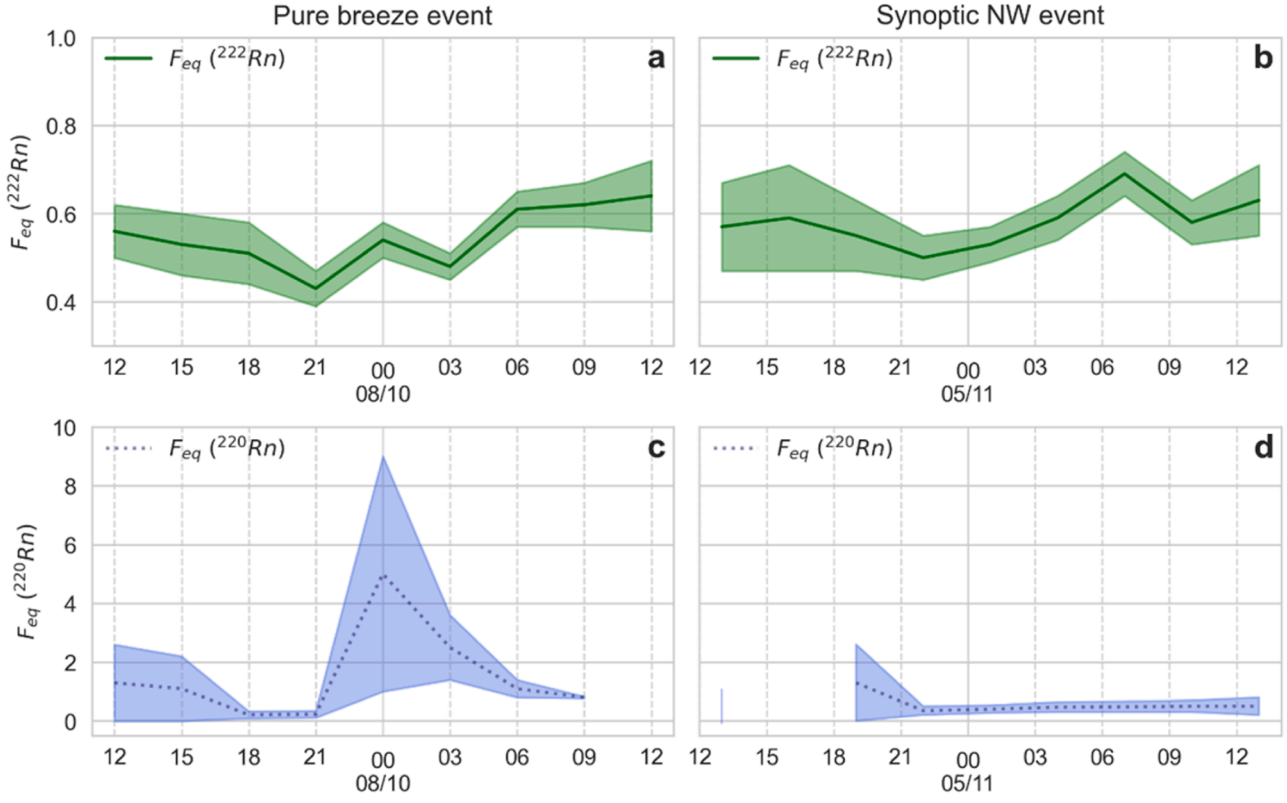

Fig. 8. Equilibrium factors (F_{eq}) for ^{222}Rn (a, b) and ^{220}Rn (c, d) for the pure breeze event (a, c) and the synoptic NW event (b, d).

studied in Section 3.2, since $F_{eq}(^{222}Rn)$ is directly proportional to the activity ratios of ^{214}Pb and ^{214}Bi with ^{222}Rn.

Regarding $F_{eq}(^{220}Rn)$, the average $F_{eq}(^{220}Rn)$ measured during the pure breeze and the synoptic NW events was 1.6(5) and 0.67(15), respectively. For $F_{eq}(^{220}Rn)$, relatively high uncertainties were obtained for both cases (31% and 22%, respectively). However, these deviations from the averages are caused by the complexity of the ^{220}Rn measurement, and they are not due to a significant temporal dependence of $F_{eq}(^{220}Rn)$. This is in line with the $^{212}Pb/^{220}Rn$ activity ratios (see Section 3.2), since, in order to calculate $F_{eq}(^{220}Rn)$, the $^{212}Pb/^{220}Rn$ activity ratio is the most relevant term of the $F_{eq}(^{220}Rn)$ equation. Consequently, $F_{eq}(^{220}Rn)$ and the $^{212}Pb/^{220}Rn$ activity ratio follow a very similar behavior.

In addition, all the values obtained for $F_{eq}(^{222}Rn)$ and $F_{eq}(^{220}Rn)$ were statistically compatible with ≤ 1, which is consistent with the findings of previous works [11,30-32]. Furthermore, in the case of the pure breeze process, the average $F_{eq}(^{222}Rn)$ of 0.55(2) agrees well with that achieved by Barba-Lobo et al. [11], 0.620(18). In addition, for the pure breeze situation, the average $^{214}Bi/^{214}Pb$ activity ratio was 0.55(4) (see Section 3.2), which also agrees well with that obtained by Barba-Lobo et al. [11], 0.50(3). This is consistent since when carrying out the air aerosol samplings shown in Barba-Lobo et al. [11], the meteorological condition present was also of breeze process type. The wind direction and speed found for the meteorological situation present for the samplings carried out by Barba-Lobo et al. [11] followed the same patterns than those found by Adame et al. [17], where a pure breeze process was also considered. See Fig. C.1 (in Supplementary Material, Appendix C) for further information about the temporal evolution of the wind direction and speed corresponding to the meteorological situation present for the samplings carried out by Barba-Lobo et al. [11].

See Tables A.4 and A.8 (in Supplementary Material, Appendix A) for further information about both Rn daughters' equilibrium factors ($F_{eq}(^{222}Rn)$ and $F_{eq}(^{220}Rn)$) obtained for each sampling carried out during the first and second 24 h cycle, respectively.

4. Summary and conclusions

The central aim of this study was to analyze the temporal evolution of radon, thoron and their respective progenies along daily cycles for two different meteorological situations (pure breeze and NW synoptic events). In addition, the atmospheric aerosol residence times and Rn daughters' equilibrium factors were analyzed for each sampling carried out along the two daily cycles.

The following main conclusions were drawn from this study:

1. Significant differences in concentrations of radon, thoron and their progenies were found between the two meteorological situations. These differences were explained by using the different values reached by the meteorological variables of interest (T, ABL height, WS and WD), obtaining much higher concentrations of these radionuclides for the pure breeze event.
2. Negative correlations were found between T and the concentrations of radon, thoron and their progenies.
3. Then, in the case of WD, two sets of concentrations of radionuclides were found for the pure breeze event: 1. WD = 0–45° (inland), for which the highest concentrations were found; and 2. WD = 180–270° (offshore), for which the concentrations were lower. However, in the case of the synoptic event, only a single set of concentrations was found, since WD = 315–360° (i.e., inland in every moment).
4. For each meteorological situation, the activity ratios of the different couples of radionuclides remained very uniform during the same sampling cycle. However, these activity ratios were significantly different ($p = 0.05$) between both meteorological situations which is consistent as proven in this study.
5. The aerosols residence times (T_r) based on radionuclides activity ratios obtained for both meteorological situations were ranged from 1 h to 3 h, which is consistent with previous studies. Then, the T_r estimated for each sampling were similar to other T_r obtained for the same sampling cycle, while they were statistically not compatible between the two different meteorological situations. This is in agreement with the results found for the activity ratios during both daily cycles. In the case of the Rn daughters' equilibrium factors, they were statistically compatible with ≤ 1 for all the cases, as expected.

CRediT authorship contribution statement

A. Barba-Lobo: Conceptualization, Data curation, Formal analysis, Investigation, Methodology, Validation, Writing – original draft, Writing – review & editing. **I. Gutiérrez-Álvarez:** Conceptualization, Data curation, Formal analysis, Investigation, Writing – original draft, Writing – review & editing. **J.A. Adame:** Conceptualization, Data curation, Formal analysis, Investigation, Writing – original draft, Writing – review & editing. **E.G. San Miguel:** Conceptualization, Data curation, Formal analysis, Investigation, Writing – original draft, Writing – review & editing. **J.P. Bolívar:** Conceptualization, Data curation, Formal analysis, Investigation, Methodology, Validation, Writing - original draft, Writing - review & editing.

Declaration of Competing Interest

The authors declare that they have no known competing financial interests or personal relationships that could have appeared to influence the work reported in this paper.

Data availability

Data will be made available on request.

Acknowledgments

This research was partially funded by the University of Huelva and the Operative FEDER Program-Andalusia 2014–2020 (Refs.: UHU-1255876, and UHU-202020), the European Regional Development Fund through the Research State Agency (Ref.: PID2020-116461RB-C21), the Andalusian Government (Ref.: PY20_00096), and the CSN (Nuclear Safety Council) projects with Refs.: SUBV-4/2022 (CLIMATOR) and SUBV-4/2021 (EXRADON).

Appendix A. Supporting information

Supplementary data associated with this article can be found in the online version at doi:10.1016/j.jhazmat.2023.132998.

References

[1] Porstendörfer, J., 1994. Properties and behaviour of radon and thoron and their decay products in the air. J Aerosol Sci 25, 219–263. https://doi.org/10.1016/0021-8502(94)90077-9.
[2] UNSCEAR, 2000. Sources and Effects of Ionizing Radiation United Nations Scientific Committee on the Effects of Atomic Radiation.
[3] Zhang, K., Feichter, J., Kazil, J., Wan, H., Zhuo, W., Griffiths, A.D., et al., 2011. Radon activity in the lower troposphere and its impact on ionization rate: a global estimate using different radon emissions. Atmos Chem Phys 11, 7817–7838. https://doi.org/10.5194/acp-11-7817-2011.
[4] Abdelfatah Mostafa, M.Y., Bader Khalaf, H.N., Zhukovsky, M., 2020. Radon decay products equilibrium at different aerosol concentrations. Appl Radiat Isot 156, 108981. https://doi.org/10.1016/j.apradiso.2019.108981.
[5] Abdo, M.A.S., Boukhair, A., Fahad, M., Ouakkas, S., Arhouni, F.E., Hakkar, M., et al., 2021. Estimation of unattached and aerosol-attached activities of airborne

short-lived radon progeny in indoor environments. J Environ Radioact 237, 106665. https://doi.org/10.1016/j.jenvrad.2021.106665.
[6] Yu, K.N., Lau, B.M.F., Nikezic, D., 2006. Assessment of environmental radon hazard using human respiratory tract models. J Hazard Mater 132, 98–110. https://doi.org/10.1016/j.jhazmat.2005.11.087.
[7] Vargas, C., Stabile, L., Cardellini, F., Morawska, L., Buonanno, G., 2016. Effect of indoor-generated airborne particles on radon progeny dynamics. J Hazard Mater 314, 155–163. https://doi.org/10.1016/j.jhazmat.2016.04.051.
[8] Nader, A.F., 2019. The determination of equilibrium factor of radon and thoron using LR-115 type II detector in a selected area from Basra Governorate, Iraq. J Phys: Conf Ser 1258, 012032. https://doi.org/10.1088/1742-6596/1258/1/012032.
[9] Rangarajan, C., 1992. A study of the mean residence time of the natural radioactive aerosols in the planetary boundary layer. J Environ Radioact 15 (3), 193–206. https://doi.org/10.1016/0265-931X(92)90058-2.
[10] Lozano, R.L., Bolívar, J.P., San Miguel, E.G., García-Tenorio, R., Gázquez, M.J., 2011. An accurate method to measure alpha-emitting natural radionuclides in atmospheric filters: application in two NORM industries. Nucl Instrum Methods Phys Res Sect A: Accel, Spectrom Detect Assoc Equip 659, 557–568. https://doi.org/10.1016/J.NIMA.2011.08.006.
[11] Barba-Lobo, A., Gutiérrez-Álvarez, I., San Miguel, E.G., Bolívar, J.P., 2023. A methodology to determine ^{212}Pb, ^{212}Bi, ^{214}Pb and ^{214}Bi in atmospheric aerosols; Application to precisely obtain aerosol residence times and Rn-daughters' equilibrium factors. J Hazard Mater 445, 130521. https://doi.org/10.1016/J.JHAZMAT.2022.130521.
[12] Lozano, R.L., San Miguel, E.G., Bolívar, J.P., 2011. Assessment of the influence of in situ 210Bi in the calculation of in situ 210Po in air aerosols: implications on residence time calculations using 210Po/210Pb activity ratios. J Geophys Res: Atmos 116, 8206. https://doi.org/10.1029/2010JD014915.
[13] Baskaran, M., 2011. Po-210 and Pb-210 as atmospheric tracers and global atmospheric Pb-210 fallout: a review. J Environ Radioact 102, 500–513.
[14] Butterweck, G., Reineking, A., Kesten, J., Porstendörfer, J., 1994. The use of the natural radioactive noble gases radon and thoron as tracers for the study of turbulent exchange in the atmospheric boundary layer—Case study in and above a wheat field. Atmos Environ 28, 1963–1969. https://doi.org/10.1016/1352-2310(94)90465-0.
[15] Sukanya, S., Noble, J., Joseph, S., 2022. Application of radon (222Rn) as an environmental tracer in hydrogeological and geological investigations: an overview. Chemosphere 303, 135141. https://doi.org/10.1016/j.chemosphere.2022.135141.
[16] Csondor, K., Erőss, A., Horváth, Á., Szieberth, D., 2017. Radon as a natural tracer for underwater cave exploration. J Environ Radioact 173, 51–57. https://doi.org/10.1016/j.jenvrad.2016.10.020.
[17] Adame, J.A., Serrano, E., Bolívar, J.P., de la Morena, B.A., 2010. On the tropospheric ozone variations in a coastal area of Southwestern Europe under a Mesoscale Circulation. J Appl Meteorol Climatol 49, 748–759. https://doi.org/10.1175/2009JAMC2097.1.
[18] Adame, J.A., Bolívar, J.P., de la Morena, B.A., 2010. Surface ozone measurements in the southwest of the Iberian Peninsula (Huelva, Spain). Environ Sci Pollut Res 17, 355–368. https://doi.org/10.1007/s11356-008-0098-9.
[19] V. Valkovic., editor, Radioactivity in the Environment: Physicochemical Aspects and Applications; 2000 1st ed, Croatia; Elsevier.
[20] Canberra Industries.Genie 2000 Spectroscopy software: Customization tools. Printed in the United States of America; 2004.
[21] Barba-Lobo, A., Bolívar, J.P., 2023. A new efficiency calibration methodology for different atmospheric filter geometries by using coaxial Ge detectors. Air Qual Atmos Health 16, 1207–1214. https://doi.org/10.1007/s11869-023-01336-x.
[22] Grossi, C., Arnold, D., Adame, J.A., López-Coto, I., Bolívar, J.P., De La Morena, B. A., et al., 2012. Atmospheric 222Rn concentration and source term at El Arenosillo 100 m meteorological tower in southwest Spain. Radiat Meas 47, 149–162. https://doi.org/10.1016/j.radmeas.2011.11.006.
[23] Gutiérrez-Álvarez, I., Guerrero, J.L., Martín, J.E., Adame, J.A., Vargas, A., Bolívar, J.P., 2021. Radon transport events associated with the impact of a NORM repository in the SW of Europe. Environ Pollut 289, 117963. https://doi.org/10.1016/J.ENVPOL.2021.117963.
[24] Gutiérrez-Álvarez, I., Guerrero, J.L., Martín, J.E., Adame, J.A., Vargas, A., Bolívar, J.P., 2019. Radon behavior investigation based on cluster analysis and atmospheric modelling. Atmos Environ 201, 50–56. https://doi.org/10.1016/j.atmosenv.2018.12.010.
[25] Vargas, A., Arnold, D., Adame, J.A., Grossi, C., Hernández-Ceballos, M.A., Bolívar, J.P., 2015. Analysis of the vertical radon structure at the spanish "El arenosillo" tower station. J Environ Radioact 139, 1–17. https://doi.org/10.1016/j.jenvrad.2014.09.018.
[26] Draxler R., Stunder B., Rolph G., Stein A., Taylor A., 2021. HYSPLIT4 User's Guide.
[27] Hersbach, H., Bell, B., Berrisford, P., Hirahara, S., Horányi, A., Muñoz-Sabater, J., et al., 2020. The ERA5 global reanalysis. Q J R Meteorol Soc 146, 1999–2049. https://doi.org/10.1002/qj.3803.
[28] Veleva, B., Valkov, N., Batchvarova, E., Kolarova, M., 2010. Variation of short-lived beta radionuclide (radon progeny) concentrations and the mixing processes in the atmospheric boundary. Environ Tracers 101, 538–554. https://doi.org/10.1016/j.jenvrad.2009.08.008.
[29] Marcazzan, G.M., Caprioli, E., Valli, G., Vecchi, R., 2003. Temporal variation of 212Pb concentration in outdoor air of Milan and a comparison with 214Bi. J Environ Radioact 65, 77–79. https://doi.org/10.1016/S0265-931X(02)00089-9.
[30] Chen, J., Harley, N.H., 2018. A review of indoor and outdoor radon equilibrium factors—part I: 222Rn. Health Phys 115, 490. https://doi.org/10.1097/HP.0000000000000909.
[31] Chen, J., Harley, N.H., 2018. A review of indoor and outdoor radon equilibrium factors-part II: 220Rn. Health Phys 115, 500–506. https://doi.org/10.1097/HP.0000000000000910.
[32] Pontedeiro, EM, Heilbron, PFL, Cotta, RM, 2007. Assessment of the mineral industry NORM/TENORM disposal in hazardous landfills. Mater, First International Conference on Engineering for Waste Treatment: Beneficial Use of Waste and By-Products (WasteEng2005) 139, pp. 563–56. ⟨https://doi.org/10.1016/j.jhazmat.2006.02.063⟩.